Motion Correction in Magnetic Resonance Imaging

Jakob M. Slipsager[1,2,3]

[1] DTU Compute, Technical University of Denmark, Kongens Lyngby, Denmark
[2] Dept. of Clinical Physiology, Nuclear Medicine & PET, Rigshospitalet, University of Copenhagen, Denmark
[3] Tracinnovations, Ballerup, Denmark

Abstract. Involuntary patient motion is an ongoing problem in magnetic resonance imaging (MRI) as motion impairs the diagnostic quality of the affected images. As a result, it is estimated that hospitals spend more than $300,000 per scanner per year on anesthesia and on repeated MRI examinations to obtain images with sufficient diagnostic quality. This note goes through some of the proposed methods to monitor head motion during an MRI scan. A state-of-the-art markerless motion tracking system is described in more detail, afterward. The note includes a short section about MRI image acquisition to better understand the concepts behind motion correction. Finally, this note goes through different motion correction methods, both Prospective and Retrospective correction.

Keywords: Motion Correction· Motion Tracking· MRI

1 Learning Objectives

- Explain why patient motion is a major problem in MRI
- Give an overview of the existing motion mitigation and correction strategies.
- Give an overview of the existing motion tracking strategies.
- In brief describe the main concepts of k-space sampling and image reconstruction.
- Describe the concepts of markerless motion tracking
- Describe the concepts of retrospective motion correction.

2 Introduction

Magnetic resonance imaging (MRI) is an important imaging modality for patient diagnosis and research. MRI non-invasively provides 3D images with high soft-tissue contrast without using ionizing radiation, which is especially important for examinations of children. Therefore, MRI is a very popular imaging modality with more than 35000 scanners installed in hospitals around the world. However, MRI requires long acquisition times compared to computed tomography (CT),

and patients need to lie still in a narrow and often loud scanner bore. A typical brain examination includes 4 to 6 imaging sequences[4], each taking 2 to 6 minutes, requiring the patient to lie in the scanner for more than 20 minutes. Such long examinations can make MRI an uncomfortable and stressful experience for the patients. Due to the long acquisition times and uncomfortable environment, patient head motion is a major concern in brain MRI, as motion impairs the diagnostic quality of the images. This effect is seen in Fig. 1 for different levels of motion. Low-quality images make the interpretation more difficult and increase the risk that the radiologist may overlook key diagnostic features. In the clinic, repeating one or more sequences is often necessary to obtain useful images. However, this strategy prolongs the examination time, causing reduced patient comfort and patient throughput. Andre et al. [1] estimated that the annual extra cost of repeating motion degraded sequences is approximately $115,000 per scanner. In pediatric MRI examinations, sedation or anesthesia are commonly used to mitigate motion, but these methods are associated with increased health risk and cost [2,3]. The added cost of anesthesia in MRI was in a recent study estimated to $319,000 per scanner per year [4].

It is not only in the clinic, involuntary patient motion is a major problem, but also in research scans of cooperative volunteers. As an example, ultra-high-resolution research scans are so sensitive that the image quality is reduced by respiratory motion. This is illustrated in Fig. 2, where the left image is corrupted by respiratory motion, while the right image is motion free.

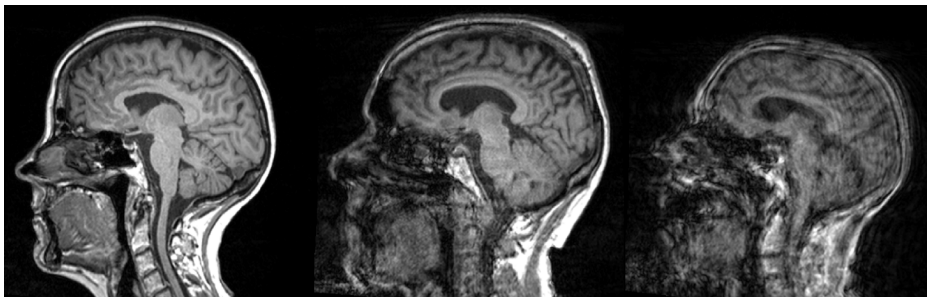

Fig. 1: Sagittal slices from MPRAGE sequences corrupted by minimal (left), moderate (middle), and large (right) motion. The left image is optimal for diagnostic use, while the middle image can be used for diagnostic, but is not optimal. The image to the right is not usable and needs to be repeated [4].

To reduce the negative impact of head motion, several motion mitigation techniques have been proposed [6,7]. The most straightforward approach is to use fast or accelerated imaging sequences [8,9] to reduce patient discomfort and

[4] An MRI sequence is a particular list of radio waves and gradient pulses used in the scanner to acquire an image.

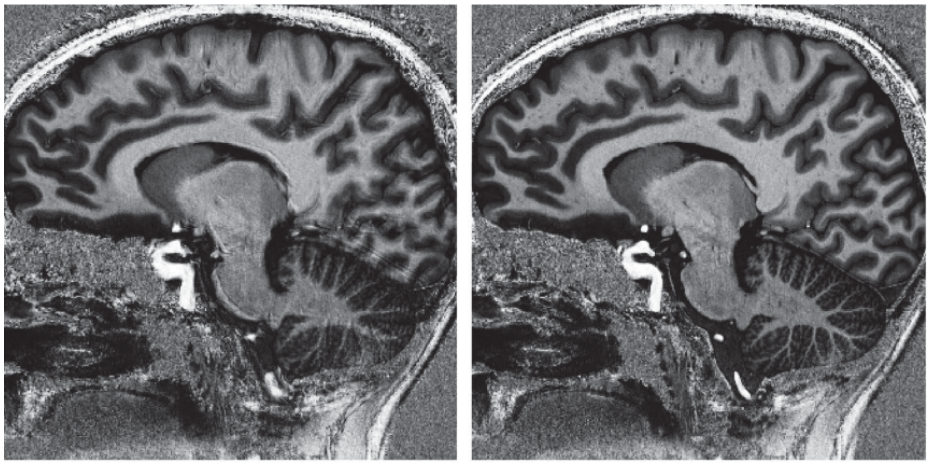

Fig. 2: Sagittal slices from a MP2RAGE sequence with a 0.5mm isotropic resolution. Left. image corrupted by motion. Right. motion free image [5]. The effect of respiratory motion is clearly seen when comparing the cerebellum in both images.

the risk of motion during the scan. Other approaches are head fixation using pads and motion robust sequences [10] utilizing (non-Cartesian) sampling strategies that are less sensitive to motion. Frequently, these motion mitigation methods are not sufficient to provide the image quality needed. Therefore, more advanced motion correction (MoCo) techniques have been developed. These methods are introduced in Section 5.

3 Estimation of Head Motion

Several of the introduced MoCo methods in Section 5 depend on accurate estimates of the patient's head motion in order to perform the correction. A variety of motion tracking approaches have been proposed. The different motion tracking approaches can be divided into internal and external tracking systems. Internal tracking systems such as navigators [11,12,13,14] estimate motion using the scanner itself with no need for additional hardware. In general, navigators are ultra short MRI sequences there can acquire images in the millisecond range. These special sequences are executed when there are available time in the host sequence (sequence acquiring the high resolution image). Patient motion is determined by comparing the current acquired navigator image with the previous using e.g. image registration. External tracking systems use additional hardware in form of e.g. cameras, light sources, and markers to estimate motion, making external tracking systems scanner independent [15,16,17,18,19]. Both types of tracking methods come with their own benefits and trade-offs. Internal systems add complexity to the acquisition, may add additional scan time, and have a

lower temporal and spatial resolution compared to external systems, meaning that motion estimates are less frequently available for MoCo compared to external tracking systems. Due to scanner independence, external tracking systems are able to provide motion estimates with a high temporal resolution to every MRI sequence. However, since these systems are independent add-on devices they must be temporal and spatial calibrated (Cross-calibration) to match the coordinate system of the scanner.

3.1 Markerless Motion Tracking

The high temporal resolution of external tracking system can results in notable higher image quality of MoCo compared to MoCo using internal tracking. However, the majority of the external systems measure motion by tracking markers attached to the patient's head. It is paramount that the markers cannot move relative to the head, otherwise, it is the movement of the markers that are estimated. Therefore, the marker attachment is a slow process, which makes these external tracking systems less suitable for clinical applications.

Markerless motion tracking records head motion without any markers attached to the patient and the setup procedure therefore is faster than the marker based system. This lecture note describes the Tracoline (TCL) markerless motion tracking system introduced in [20]. The TCL system is an external device with its electronics placed behind the scanner in a radio frequency shielded box (see Fig. 3a). The system optics (vision probe) is mounted to the scanner table and has visibility of the patient's face through the openings in the head coil (Fig. 3b). Optical fibers transfer light between the vision probe and system electronics. The TCL system projects near-infrared structured light on the face of the patient to reconstruct 3D point clouds of the face at a rate of 30 point clouds per second. Each point in the point cloud acts like a marker attached to the face and the head motion is estimated by finding the motion between corresponding markers in a current and in a reference point cloud. This is achieved by continuously performing rigid-body registrations using the iterative closest point (ICP) algorithm, between the currently generated and the initially acquired point cloud. This is illustrated in Fig. 4, where the point cloud in blue is the reference. The lines illustrate 10 random selected point correspondences estimated with ICP. The head motion is encoded in the 4x4 transformation matrix $\mathbf{T}(t)$ determined in the registration that aligns the two point clouds. An example of acquired head motion is shown in Fig. 5.

3.2 Cross-Calibration

In external tracking systems, the recorded motion is defined in the tracking device's coordinate system (tcs). It is necessary to transform the tracking data into the scanner's coordinate system (scs) before it can be used for MoCo. This procedure is known as the cross-calibration and it consists of a temporal and a geometric calibration between tracking device and scanner. The cross-calibration

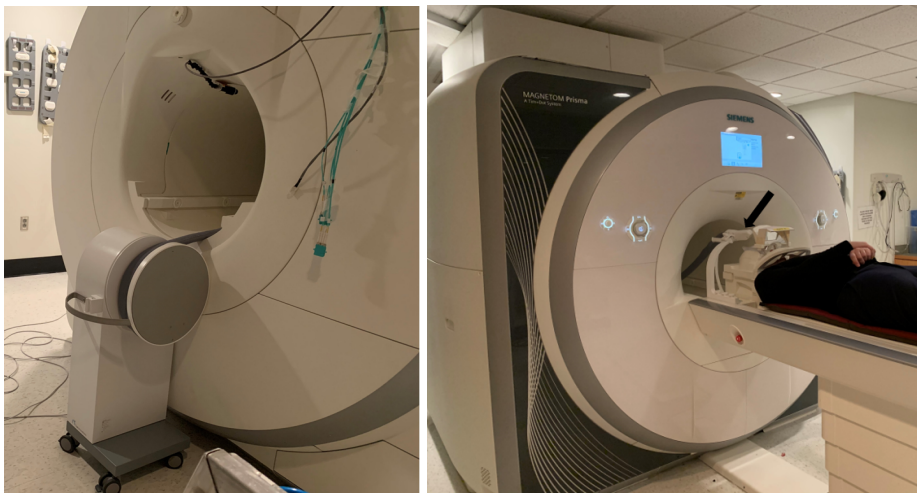

(a) System electronics (b) Vision probe

Fig. 3: The setup of the TCL system on the MRI scanner. The arrow is pointing on the TCL system's optics (vision probe). The vision probe is mounted to the scanner table to have sufficient visibility of the patient's face through the openings in the head coil.

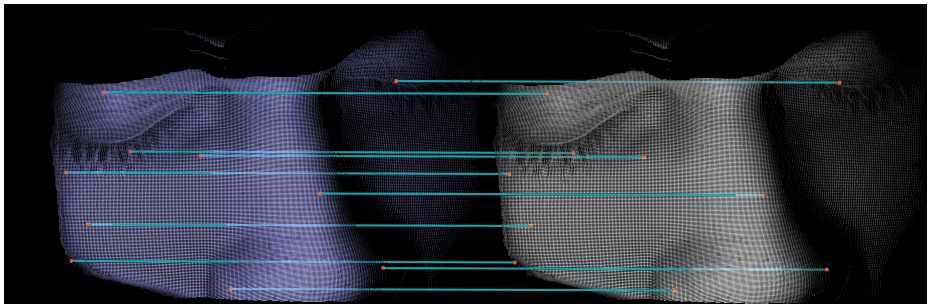

Fig. 4: Alignment of a surface scan (Right) to the reference surface (Left) using iterative closest point (ICP). The lines represent 10 random selected point correspondences between the two surfaces.

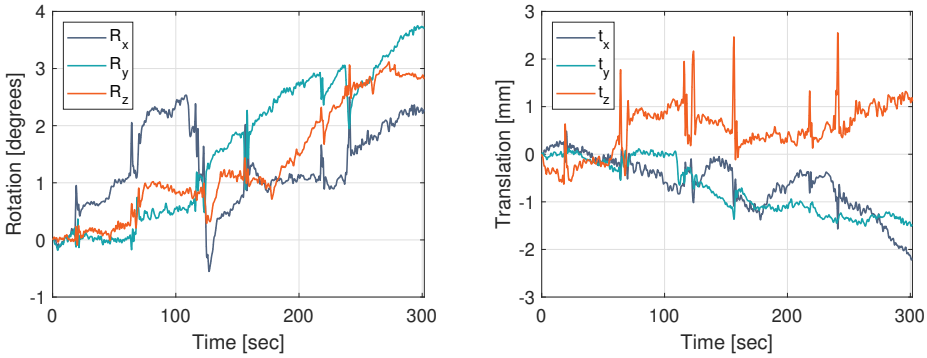

Fig. 5: Head motion acquired during a 5 minute long clinical MRI sequence.

is carried out differently among the external tracking systems. In the TCL system, the geometric calibration is performed by extracting a point cloud of the patient's head, from a special calibration scan on the scanner. This point cloud is defined in the scs, since it is extracted from an MRI image. The geometric transformation ${}_{scs}\mathbf{A}_{tcs}$ that map between tcs and scs is determined by aligning a point cloud from the tracking device to the point cloud from the scanner. The ICP algorithm is used to perform the alignment. The motion defined in tcs ${}_{tcs}\mathbf{T}_{tcs}(t)$ are transformed to scs by

$$ {}_{scs}\mathbf{T}_{scs}(t) = {}_{scs}\mathbf{A}_{tcs}\, {}_{tcs}\mathbf{T}_{tcs}(t)\, {}_{scs}\mathbf{A}_{tcs}^{-1} \tag{1} $$

The temporal calibration is performed by a network time synchronization between the scanner and tracking computer.

4 MRI Image Acquisition

An MRI scanner uses a powerful magnet to create a static magnetic field B_0 with a strength of several Tesla. When a patient is placed inside the scanner, the magnetic hydrogen nuclei in the body will start to point in the same direction as B_0 and precess around the field at a certain frequency f_0 (Larmor frequency). Radio waves with a frequency equal to f_0 and perpendicular to B_0 are used to push the hydrogen nuclei away from their precession around B_0. In the seconds after the radio waves have been turned off, the nuclei will emit weak radio waves. These radio waves are measured with coils around the patients and the measured signals are what eventually become the MRI image. To determine spatial localization of the emitted radio waves, the scanner uses imaging gradients G_x, G_y, and G_z to create linear variations in B_0. The scanner does not spatial encode the entire image at once as a regular camera, instead, it measures the spatial frequency components of the image one line of frequencies at a time. The frequency representation of an image is within the MRI community called the K-space and it is equivalent to the Fourier-space. In practice, the k-space

representation of an image is a similar sized array of complex numbers. Each pixel value at a given spatial frequency $\mathbf{k} = [k_x, k_y, k_z]^T$ contains information about the frequency and phase of every pixel in the corresponding image. As an example, a pixel near the k-space center ($\mathbf{k} = [0, 0, 0]^T$) contains information about the low-frequency components of the image, which could e.g. be large objects with homogeneous intensities. The majority of the scanned objects consist mostly of large homogeneous objects (e.g. white brain matter) and this is why the center of k-space often is the brightest area (see Fig. 6b).

An MRI sequence is a particular combination of radio wave pulses and imaging gradients. One of the major workhorses in brain MRI is a Magnetization Prepared - RApid Gradient Echo (MPRAGE) sequence. The sequence diagram in Fig. 6a illustrates how an MPRAGE sequence manipulates the static B_0-field in order to sample k-space. The first row in the diagram shows the applied radio wave pulses to create the desired MRI signal and contrast. The remaining rows show the activation-time and amplitude of the imaging gradients. The MPRAGE sequence populates the 3D K-space through an inner and an outer loop. The inner loop, samples frequency components in the k-space plane spanned by the k_z, and the k_y axes as illustrated in Fig. 6b. The first line is sampled by applying a positive y-gradient in combination with a negative z-gradient to move from the origin to the top left corner in k-space (Dashed line). Then a readout is performed by applying a positive z-gradient while data are measured. This procedure is repeated with a gradual lower G_y until the entire k-space plan is sampled. The amplitude of G_x is varied in the outer loop in order to go through all planes. The k-space sampling process takes several minutes to complete, depending on the resolution. Patient motion during this period may result in artifacts in the final image due to inconsistency between various portions of the sampled k-space data [6].

The final image is reconstructed by an inverse Fourier transformation of the sampled k-Space. In the majority of the clinical sequences, k-space is sampled on a Cartesian grid as in Fig. 6b to simplify the reconstruction, by using the inverse fast Fourier transformation.

5 Motion Correction

As mentioned in the introduction, many different motion correction solutions have been proposed. Overall, these methods can be divided into Prospective MoCo and Retrospective MoCo. However, methods combining concepts from both Prospective and Retrospective MoCo have been suggested too.

5.1 Prospective Motion Correction

Prospective motion correction (ProMoCo) is a group of methods, where the correction is performed in real-time during the scan. ProMoCo is performed by continuously updating the scanners field of view (FOV) to follow a moving object (e.g. a patient's head), as illustrated in Fig. 7. Special ProMoCo sequences

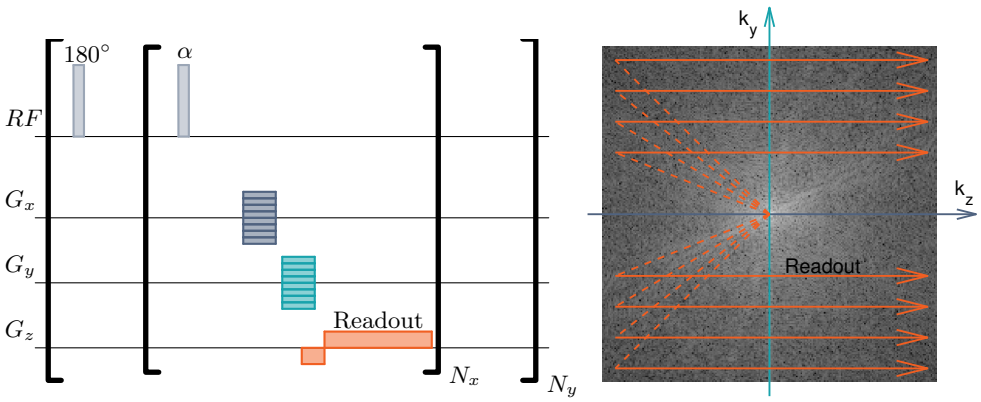

(a) MPRAGE Sequence (b) K-Space Sampling

Fig. 6: (a) Diagram of an MPRAGE sequence. The first row shows the radio frequency (RF) pules, while the remaining shows the amplitude of x, y and, z imaging gradients (G_x, G_y, and G_z). (b) Illustration of how K-space is sampled.

are designed to receive motion estimates and then update the FOV by adjusting the imaging gradients before doing a readout. The methods mentioned in Section 3 can be used to estimate the motion of the scanned object and send this information to the ProMoCo sequence.

5.2 Retrospective Motion Correction

Retrospective motion correction (RetroMoCo) takes place after the scan when all the data have been acquired. Many different methods within the field of RetroMoCo exist and they can be divided into 2 groups based on where the correction takes place.

Correction in Image Domain In the first group, the correction takes place in the image domain after the image has been reconstructed. These methods can e.g. utilize intensity-based image registration to realign images to their correct positions. This type of RetroMoCo is often applied on a time series of images as in functional MRI. The intensity-based image registrations can also be replaced by transformations estimated using motion tracking systems as done in [21].

In recent years, several MoCo approaches within the field of deep learning have been proposed. The common strategy is to pass the motion corrupted MRI image through a trained encoder-decoder network to perform the MoCo. The MoCo network is often trained on motion corrupted images synthetic generated based on motion-free images. The training process is conducted by updating the network parameters based on a calculated loss between the motion free image and the corrected image (network output).

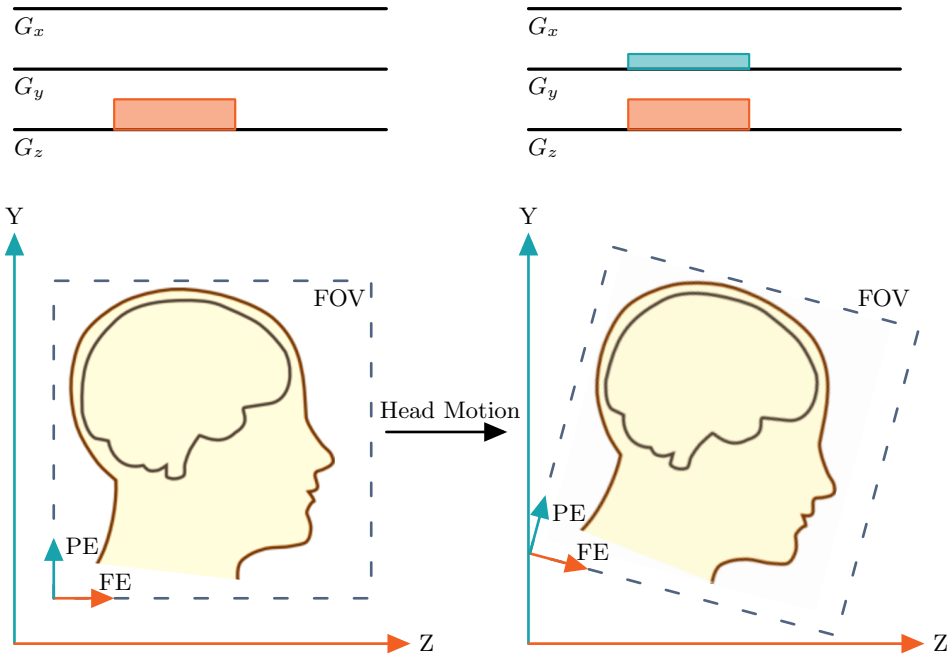

Fig. 7: Illustration of how prospective motion correction adjusts the imaging gradients (G_x, G_y, and G_z) in order to change the Field of View (FOV) to follow a moving head. The left column illustrates the situation before head motion, while the right column shows how the scanner responses to head motion.

Correction in K-Space Domain In retrospective correction of K-space, the goal is to reposition individual k-space sub-regions according to the occurred motion when the sub-regions were sampled. These sub-regions are e.g. lines or entire planes of the acquired k-space and contain multiple data points. The k-space reposition can be driven by the data itself or by external knowledge about the motion. The data-driven methods work by iteratively correcting the acquired sub-regions to optimize quality measures (e.g. entropy or gradient entropy)[22].

This note describes the pipeline introduced in [23] to correct K-space using prior knowledge about the motion. The first step in the pipeline is to transform the recorded motion into the coordinate system of the scanner by

$$_{scs}\mathbf{T}_{scs}(t) =_{scs} \mathbf{A}_{tcs}\, _{tcs}\mathbf{T}_{tcs}(t)\, _{scs}\mathbf{A}_{tcs}^{-1} \tag{2}$$

, where $_{scs}\mathbf{A}_{tcs}$ is the cross calibration between the motion tracking system and the scanner. The second step is to assign the nearest recorded motion estimate in time to each sub-region as illustrated in Fig. 8a. Then every k-space sub-region r is assigned a matrix $_{scs}\mathbf{T}_{scs}(r)$ that encodes the patient's head position relative to a reference position when the sub-region was sampled. Each assigned matrix $_{scs}\mathbf{T}_{scs}(r)$ is a 4x4 transformation matrix with the form

$$_{scs}\mathbf{T}_{scs}(r) = \begin{bmatrix} \mathbf{R}_r & & \mathbf{t}_r \\ 0 & 0\,0 & 1 \end{bmatrix}, \tag{3}$$

where $\mathbf{R}_r$ is a 3x3 rotation matrix and $\mathbf{t}_r$ is a vector containing the three translations. In the third step, sub-regions are transformed by the assigned translation parameters. This is done by adding additional phase shifts to the acquired k-space values $I_{ksp}(\mathbf{k}_{i,r})$ by

$$\hat{I}_{ksp}(\mathbf{k}_{i,r}) = I_{ksp}(\mathbf{k}_{i,r})\mathrm{e}^{-i\pi(\mathbf{k}_{i,r}\mathbf{t}_r)} \tag{4}$$

, where $\hat{I}_{ksp}$ is the phase shifted value and $\mathbf{k}_{i,r}$ is the i'th k-space position within the r'th k-space sub-region. In the fourth step, every k-space position $\mathbf{k}_{i,r}$ in all the sub-regions are transformed by the assigned rotations by

$$\hat{\mathbf{k}}_{i,r} = \mathbf{k}_{i,r}\mathbf{R}_r \tag{5}$$

,where $\hat{\mathbf{k}}_{i,r}$ is the the rotated k-space position. The rotated k-space sub-regions is illustrated in Fig. 8b. After the reposition of the sub-regions, the k-space is no longer uniformly sampled and thus the inverse non-uniform fast Fourier transformation is used to reconstruct the corrected image (see Fig. 8d).

The main advantage with RetroMoCo compared to ProMoCo is illustrated in Fig. 8c. Namely that the uncorrected image can be preserved by reconstructing the image before the k-space is corrected. This is not possible in ProMoCo since the data is corrected while it is acquired.

In Fig. 9, the explained RetroMoCo method was used to correct the motion corrupted MPRAGE scan in (A). The results of the correction is shown in (B).

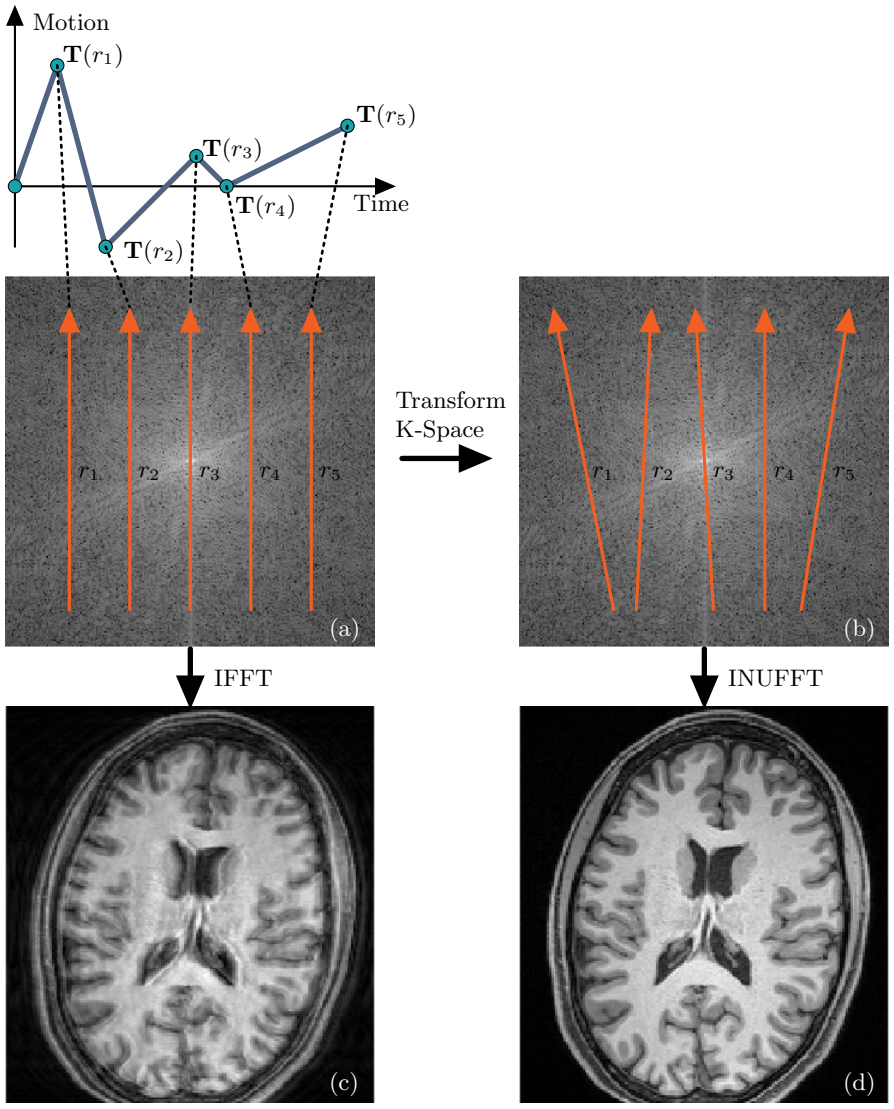

Fig. 8: Illustration of the retrospective motion correction (RetroMoCo) pipeline. (a) Each K-space readout r is assigned with the nearest motion estimate $\mathbf{T}(r)$. (b) K-Space is updated according to the assigned motion estimates by rotations and phase shifts. (c) The uncorrected image is reconstructed by an inverse fast Fourier transformation (IFFT) of the original k-space. (d) The RetroMoCo image is reconstructed by an inverse non-uniform fast Fourier transformation (INUFFT) of the corrected k-space.

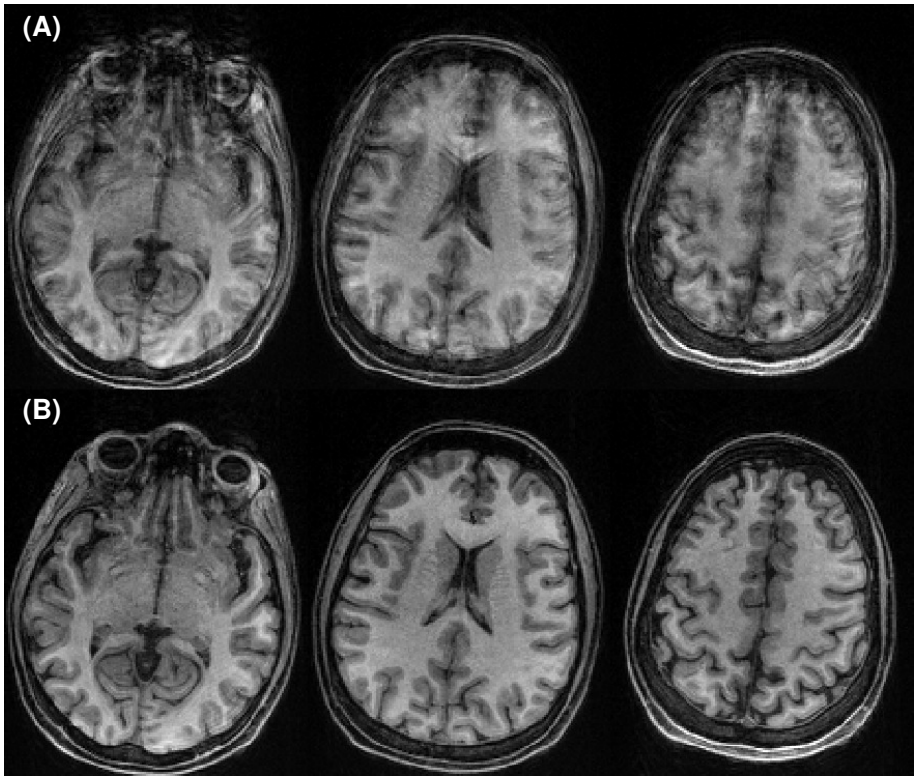

Fig. 9: Axial slices of an MPRAGE scan reconstructed with and without retrospective motion correction. (A) Uncorrected slices. (B) corrected slices

References

1. J. B. Andre, B. W. Bresnahan, M. Mossa-Basha, M. N. Hoff, C. Patrick Smith, Y. Anzai, and W. A. Cohen, "Toward quantifying the prevalence, severity, and cost associated with patient motion during clinical MR examinations," *Journal of the American College of Radiology*, vol. 12, no. 7, pp. 689–695, 2015.
2. R. D. Sanders, J. Hassell, A. J. Davidson, N. J. Robertson, and D. Ma, "Impact of anaesthetics and surgery on neurodevelopment: An update," *British Journal of Anaesthesia*, vol. 110, pp. 53–72, 2013.
3. D. Blumenthal and M. Tavenner, "Anesthesia and Developing Brains — Implications of the FDA Warning," *The New England Journal of Medicine*, vol. 376, no. 10, pp. 905–907, 2017. [Online]. Available: http://scholar.google.com/scholar?hl=en{&}btnG=Search{&}q=intitle:New+engla+nd+journal{#}0
4. J. M. Slipsager, S. L. Glimberg, J. Søgaard, R. R. Paulsen, H. H. Johannesen, P. C. Martens, A. Seth, L. Marner, O. M. Henriksen, O. V. Olesen, and L. Højgaard, "Quantifying the Financial Savings of Motion Correction in Brain MRI : A Model-Based Estimate of the Costs Arising From Patient Head Motion and Potential Savings From Implementation of Motion Correction," *Journal of Magnetic Resonance Imaging*, pp. 1–8, 2020.
5. F. Gretsch, H. Mattern, D. Gallichan, and O. Speck, "Fat navigators and Moiré phase tracking comparison for motion estimation and retrospective correction," *Magnetic Resonance in Medicine*, vol. 83, no. 1, pp. 83–93, 2020.
6. M. Zaitsev, J. Maclaren, and M. Herbst, "Motion artifacts in MRI: A complex problem with many partial solutions," *Journal of Magnetic Resonance Imaging*, vol. 42, no. 4, pp. 887–901, jan 2015. [Online]. Available: http://dx.doi.org/10.1002/jmri.24850
7. J. Maclaren, M. Herbst, O. Speck, and M. Zaitsev, "Prospective Motion Correction in Brain Imaging: A Review," *Magnetic resonance in medicine*, vol. 69, no. 3, pp. 621–636, 2013.
8. M. K. Stehling, R. Turner, and P. Mansfield, "Echo-planar imaging: Magnetic resonance imaging in a fraction of a second," *Science*, vol. 254, no. 5028, pp. 43–50, 1991.
9. D. K. Sodickson and W. J. Manning, "Simultaneous acquisition of spatial harmonics (SMASH): Fast imaging with radiofrequency coil arrays," *Magnetic Resonance in Medicine*, vol. 38, no. 4, pp. 591–603, 1997.
10. G. E. Sarty, "Single TrAjectory Radial (STAR) Imaging," *Magnetic Resonance in Medicine*, vol. 51, no. 3, pp. 445–451, 2004.
11. D. Gallichan and J. P. Marques, "Optimizing the acceleration and resolution of three-dimensional fat image navigators for high-resolution motion correction at 7T," *Magnetic Resonance in Medicine*, vol. 77, no. 2, pp. 547–558, 2017.
12. N. White, C. Roddey, A. Shankaranarayanan, E. Han, D. Rettmann, J. Santos, J. Kuperman, and A. Dale, "PROMO: Real-time prospective motion correction in MRI using image-based tracking," *Magnetic Resonance in Medicine*, vol. 63, no. 1, pp. 91–105, 2010.
13. M. D. Tisdall, M. Reuter, A. Qureshi, R. L. Buckner, B. Fischl, and A. J. van der Kouwe, "Prospective motion correction with volumetric navigators (vNavs) reduces the bias and variance in brain morphometry induced by subject motion," *NeuroImage*, vol. 127, pp. 11–22, 2016. [Online]. Available: http://dx.doi.org/10.1016/j.neuroimage.2015.11.054

14. A. J. W. Van der Kouwe, T. Benner, and A. M. Dale, "Real-time rigid body motion correction and shimming using cloverleaf navigators," *Magnetic resonance in medicine*, vol. 56, no. 5, pp. 1019–1032, 2006.
15. J. Schulz, T. Siegert, E. Reimer, C. Labadie, J. Maclaren, M. Herbst, M. Zaitsev, and R. Turner, "An embedded optical tracking system for motion-corrected magnetic resonance imaging at 7T," *Magnetic Resonance Materials in Physics, Biology and Medicine*, vol. 25, no. 6, pp. 443–453, 2012.
16. M. Aksoy, C. Forman, M. Straka, S. Skare, S. Holdsworth, J. Hornegger, and R. Bammer, "Real-time optical motion correction for diffusion tensor imaging," *Magnetic Resonance in Medicine*, vol. 66, no. 2, pp. 366–378, 2011.
17. M. B. Ooi, S. Krueger, W. J. Thomas, S. V. Swaminathan, and T. R. Brown, "Prospective Real-Time Correction for Arbitrary Head Motion Using Active Markers," *Magnetic resonance in medicine*, vol. 62, no. 4, pp. 943–954, 2009.
18. J. M. Slipsager, A. H. Ellegaard, S. L. Glimberg, R. R. Paulsen, M. Dylan Tisdall, P. Wighton, A. Van Der Kouwe, L. Marner, O. M. Henriksen, I. Law, and O. V. Olesen, "Markerless motion tracking and correction for PET, MRI, and simultaneous PET/MRI," *PLoS ONE*, vol. 14, no. 4, pp. 1–17, 2019.
19. R. Frost, P. Wighton, F. I. Karahanoğlu, R. L. Robertson, P. E. Grant, B. Fischl, M. D. Tisdall, and A. van der Kouwe, "Markerless high-frequency prospective motion correction for neuroanatomical MRI," *Magnetic Resonance in Medicine*, vol. 82, no. 1, pp. 126–144, 2019.
20. O. V. Olesen, M. R. Jørgensen, R. R. Paulsen, L. Højgaard, B. Roed, and R. Larsen, "Structured Light 3D Tracking System for Measuring Motions in PET Brain Imaging," in *SPIE Medical Imaging*, vol. 7625. International Society for Optics and Photonics, 2010, p. 76250X.
21. R. Beckerleg, J. Whittaker, D. Gallichan, and K. Murphy, "Correcting motion registration errors caused by global intensity changes during CVR and," in *Proceedings of the 28th Annual Meeting of ISMRM*, 2020, p. 0471.
22. D. Atkinson, D. L. Hill, P. N. Stoyle, P. E. Summers, S. Clare, R. Bowtell, and S. F. Keevil, "Automatic compensation of motion artifacts in MRI," *Magnetic Resonance in Medicine*, vol. 41, no. 1, pp. 163–170, 1999.
23. D. Gallichan, J. P. Marques, and R. Gruetter, "Retrospective correction of involuntary microscopic head movement using highly accelerated fat image navigators (3D FatNavs) at 7T," *Magnetic resonance in medicine*, vol. 75, no. 3, pp. 1030–1039, 2016.